Binary collision lattice simulation study of model parameters in monocrystalline sputtering

1989 J. Phys.: Condens. Matter 1 4697

(http://iopscience.iop.org/0953-8984/1/28/019)

J. Phys.: Condens. Matter **1** (1989) 4697–4722. Printed in the UK

Binary collision lattice simulation study of model parameters in monocrystalline sputtering

J Likonen† and M Hautala‡

† Technical Research Centre of Finland, Reactor Laboratory, Otakaari 3 A, SF-02150 Espoo, Finland

‡ Department of Physics, University of Helsinki, Siltavuorenpenger 20 D, SF-00170 Helsinki, Finland

Received 11 November 1988, in final form 2 May 1989

Abstract. Cu ejection and sputtering by Ar ions have been studied in the specific case of 5 keV Ar impinging the (100), (110) and (111) surfaces using the binary collision lattice simulation code COSIPO. The influence of various parameters in treating the binary collisions has been studied. On the basis of these studies the feasibility of the binary collision lattice simulations in connection with sputtering is discussed. The effect of interaction potential on sputtering is studied by using two different potential functions for the ion–atom and atom–atom interaction potentials. The strengths of the potentials have been changed by using various screening lengths and cut-offs. To model electronic stopping both frictional and impact parameter dependent electronic energy losses are used. It is found that the angular distributions of the sputtered atoms depend mainly on the atom–atom interaction potential. The ion–atom potential and the electronic stopping have only minor effects. The yield, however, depends markedly on the inelastic energy losses and the ion–atom potential. The sensitivity of the sputtering yield on the potentials and on the parameters in treating the binary collisions as well as the influence of the simultaneous collisions depend critically on the strength of the potential. Calculations show that the dependence on these factors is weak if the strengths of the potentials are such that experimental yields are achieved. Several combinations of the interaction potentials and inelastic losses give good agreement with either experimental yields or angular distributions of sputtered particles. However, a combination exists that reproduces all the experimental results.

1. Introduction

Sputtering of atoms from solid surfaces plays an important role in many modern fields, e.g. in thin-film deposition, SIMS analysis, ion etching, high-dose ion implantation and plasma–wall interaction in fusion devices. The sputtering mechanisms from metals are well understood to be of atomic collision origin and are often described by the model of a linear transport theory (Sigmund 1969). This model is found to give reasonable results for sputtering yields from structureless materials. Some simplifying assumptions are introduced in order to allow analytical treatment of the problem, such as power law approximation to the interaction potential, the assumption of an infinite target and isotropic recoil-flux in linear cascades.

For crystalline targets, the sputtering yields are influenced by the lattice structure especially for particle incidence and emergence in close packed directions. In addition to this, the regular arrangement of atoms cannot be neglected because correlated collisions

0953-8984/89/284697+26$02.50

propagate along atomic rows effectively. The basic features of such correlated collisions were suggested first by Silsbee (1957) and Nelson *et al* (1962) extended the focusing sequence mechanism to the case of thermally vibrating atomic rows. An alternative model to the Silsbee mechanism was developed by Lehmann and Sigmund (1966). This model is based on the assumption of a random collision cascade in the bulk that encounters a surface with a periodic structure. Neither model is fully satisfactory. In recent computer simulations it has been shown that both mechanisms take place in single-crystal sputtering (Hou and Eckstein 1986, Yamamura and Takeuchi 1987). Onderdelinden (1968) suggested that at energies above a few keV, channelling will also influence the sputtering process and related the sputtering yield of a monocrystalline target to the sputtering yield of a structureless medium through some parameters.

Computer simulation is an efficient method for studying atomic collision processes in solids because many of the approximations in analytical theories can be omitted. A number of computer simulation experiments have in fact been undertaken (for reviews see Harrison 1983, 1988, Andersen 1987).

The most thoroughly studied ion–target combination is by no doubt Ar–Cu (see e.g. Nelson and Thompson 1961, Southern *et al* 1963, Robinson *et al* 1963, 1967, 1974, Fluit *et al* 1963, Magnuson and Carlston 1963, Weijsenfeld 1966, 1967, Harrison *et al* 1968 (however, see Robinson 1969, Harrison 1969), 1973, Elich *et al* 1971, 1972, Hou *et al* 1976, 1979, 1986, Andersen *et al* 1985, Karpuzov 1987, Yamamura and Takeuchi 1987, Eckstein and Hou 1988). The non-experimental papers have mainly concentrated on the comparisons with experimental data. Less emphasis has been paid on detailed studies of the influence of various technical and physical factors on the results. We have also made some studies recently on this system with a special emphasis on the qualitative features, such as the effect of the target structure on the various characteristic features in sputtering (Hautala and Likonen 1987, 1988a, b, Likonen and Hautala 1988). Now our aim is to put a more quantitative basis on the studies and to show that the quotations of Robinson and Torrens (1974) concerning the motions of low-energy particles should be taken seriously. This means that an agreement with experimental results is not a sufficient proof of the reliability of the calculations.

If quantitative comparison with experimental results is performed one should know the influence of the various parameters in the studied case in order to make definite conclusions of the physical factors present in sputtering. This has led us to rather extensive calculations where the aim has been to study separately the parameters involved in the binary collision (BC) approximation itself and the physical parameters. Ar–Cu is again chosen for the case study since there exists experimental data for both sputtering yields and angular distributions for various orientations of crystal. The accumulated data make it possible to draw conclusions on the significance of the similarity of experimental and calculated results. A hopeful situation would be that the agreement were achieved by only one set of physical parameters. In addition, the variation of the strength of the potential makes possible a discussion of the validity of theoretical arguments concerning monocrystalline sputtering.

Accordingly, §3 is directed to a detailed study of the effect of the various technical parameters in the binary collision lattice simulations and Monte Carlo calculations. We want to show that the quantitative results are rather sensitive to some model parameters and therefore one should be careful in extracting physical conclusions on the results. One should note that although we use here only the BC approximation the same is true for other methods, too. The technical parameters are always to be studied. The uncritical use of any method is less formally known by the familiar phrase

'garbage in, garbage out' (Harrison 1988).

In §4 the relative changes in sputtering yields and angular distributions due to different ion–atom and atom–atom interaction potentials and electronic energy losses are investigated. Ion means the incoming ion and atom is a target atom. No such comparison has been performed so far for several crystal orientations at a time where both the yields and angular distributions are compared and the ion–atom and atom–atom potentials are varied individually. It will be shown that by suitable selection of these factors good agreement with experimental data may be achieved even in the case of angular distributions. In fact it will be shown that both the sputtering yield and the angular distribution must be included in the study if any conclusions of the validity of the physical assumptions are wanted. A similar conclusion was recently obtained by Eckstein and Hou (1988) in the case of Xe in Au using a more limited amount of information. It will be shown that the sensitivity of the sputtering yield on the potential and the parameters in treating the collisions as well as the influence of the simultaneous collisions depend critically on the strength of the potential and that the dependence is rather weak for realistic potentials. This fact is the basis of the feasibility of the BC calculations, not any agreement with experiment.

2. Method of calculation

In these studies we have used the COSIPO code (Hautala 1984), with the following modifications and assumptions in the calculations. The values of the model parameters given below should be understood as standard ones, which have been used if not otherwise stated in the text.

In the binary collision approximation the trajectories between collisions are approximated by straight lines and the projectiles and recoils always move along the asymptotes. This results in corrections to the initial positions of the asymptotes. These corrections mean that the point of deflection of the projectile is shifted back in the laboratory system by an amount x_1 and the initial position of the recoil is moved in the forward direction along the incoming asymptote by an amount x_2. The trajectories of the colliding particles are shown in figure 1. The present version of COSIPO allows the option of limiting the maximum values of x_1 and x_2. These options permit tests of the importance of various details of the treatment of binary collisions on the overall results of the sputtering calculations. In principle large x_1, x_2 values show that the BC approximation is no longer valid; the collision cannot be treated individually, the next collision starts before the previous is accomplished. The procedure for the simultaneous collisions was modified slightly compared with the earlier one used in Hautala (1984) and Likonen and Hautala (1988). The next main scatterer is the nearest one (distance x_i) that has the impact parameter b_i less than the maximum value $b_{\max 1}$, which is half of the lattice constant $a = 3.6$ Å (see figure 1). The following collisions are treated as simultaneous with this main collision: if the impact parameter b_j is less than the maximum value $b_{\max 2}$ and the distance x_j is less than $x_i + \Delta x$. The energy losses of these collisions are included. The parameter Δx defines the distance along a trajectory of a projectile within which next successive atoms must be encountered to be considered simultaneously. The inclusion of the second maximum impact parameter $b_{\max 2}$, which is usually chosen larger than $b_{\max 1}$, improves the treatment of simultaneous collisions. A value of $0.62a$ for $b_{\max 2}$ was used as in earlier MARLOWE simulations (Hou and Robinson 1978, 1979, Karpuzov 1987, Karpuzov and Armour 1984). The parameter

Δx was chosen to be 0.4 Å. As will be seen below, this value should be large enough in order that all atoms forming more or less symmetric focusing rings are included if the main collider belongs to the ring. The deflections due to these simultaneous collisions are included only if b_j is less than $1.5b_i$. Each of the simultaneous collisions is carried out as if it were occurring alone. The several deflections of the projectile due to each collision are added vectorially.

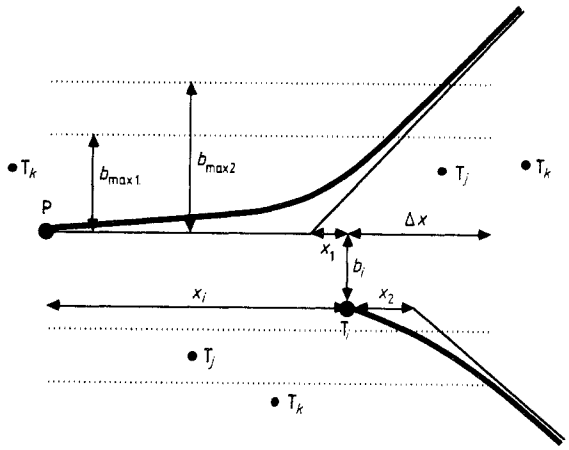

Figure 1. The trajectories of colliding particles. P is the projectile and T_i the main collider. Collisions with atoms T_j are regarded as simultaneous with T_i, whereas atoms T_k are ignored. x_1 and x_2 are the corrections to the initial positions of the asymptotes. x_i is the distance between P and T_i. b_i is the impact parameter. b_{max1} and b_{max2} are the maximum impact parameters for the main collision and for the simultaneous collisions, respectively. An atom is included in the collision only if its distance to P is less than $x_i + \Delta x$.

The simultaneous treatment used here avoids an instability into the motion of a well channelled particle, but it underestimates the energy loss. The underestimation of the energy losses by a few tenth of an eV per collisions can be noticed when the binary collision and molecular dynamics results are compared with each other (Robinson 1981). Therefore, usually an amount of $E_b = 0.2$ eV is subtracted from the kinetic energy of every atom leaving its lattice site. This is also our standard value. In addition we study the influence of its variation on the sputtering data.

The interaction potential $V(r)$ is assumed to be a screened Coulomb potential; the screening function is either the Molière function (Molière 1947) or it is a mean potential obtained by fitting a sum of exponentials to 50 ion–atom potentials obtained using Dirac–Fock calculations of the electron densities (Bister *et al* 1979). This mean potential is close to the so-called universal potential (Wilson *et al* 1977, Biersack and Eckstein 1984). The screening lengths used are Firsov a_F, Thomas–Fermi a_{TF} ($a_{TF} = 1.121a_F$ for Ar+Cu collisions, $a_{TF} = 1.123a_F$ for Cu+Cu collisions) or those suggested by Robinson (Robinson and Torrens 1974, Hou and Robinson 1978, 1979). In the latter case the screening length for the Ar+Cu collision is $0.86a_F$ and for the Cu+Cu collision $0.77a_F$. The effect of the neighbouring atoms on the scattering process was estimated with the potential (Latta and Scanlon 1974)

$$U(r) = \begin{cases} V(r) + V(2r_c - r) - 2V(r_c) & r < r_c \\ 0 & r \geq r_c. \end{cases} \tag{1}$$

$V(r)$ is either the Molière or the mean potential. The effect of the form (1) is mainly that the zero of potential occurs at $r = r_c$. Here r_c is chosen to be half of the lattice constant. Some of the potentials used in the calculations are shown in figure 2. Also the nuclear stopping powers S_n

$$S_n(E) = 2\pi N \int_0^{b_{max2}} b\Delta E_n \, db \tag{2}$$

$$\Delta E_n = [4EM_1M_2/(M_1 + M_2)^2] \sin^2(\theta/2) \tag{3}$$

are calculated from the potentials shown in figure 2. The $\theta(b)$ dependence is given by the classical scattering formula

$$\theta = \pi - 2b \int_{r_0}^{\infty} \left[r^4 \left(1 - \frac{V(r)}{E_r} - \frac{b^2}{r^2} \right) \right]^{-1/2} dr \tag{4}$$

where r_0 is the apsis of the collision and E_r is the relative kinetic energy.

In earlier sputtering calculations (Likonen and Hautala 1988) the crystal was perfect during the whole cascade calculations. In the present version of COSIPO a simple model for the erosion of the surface is included as an option. The search of next scatterers includes a check of the possibility that the atom from a lattice site has already been sputtered and therefore the site is vacant. However, as it will be shown later, the approximation of the perfect crystal seems to be good.

Inelastic energy losses are included in the calculations using the trajectory-dependent LSS theory (Lindhard *et al* 1963), the impact parameter dependent Firsov model (1959) modified by Robinson and Torrens (1974) or the Oen–Robinson loss model (Oen and Robinson 1976). In the non-local LSS theory, where the impact parameter dependence is neglected, electronic energy loss is simply obtained by

$$\Delta E_e = NLS_e(E) \tag{5}$$

where L is the distance travelled between collisions and $S_e(E)$ is the electronic stopping cross section

$$S_e(E) = kE^{1/2}. \tag{6}$$

LSS theory is valid at velocities $v < Z_1^{2/3}c/137$ in random media and it approximates well the general trends in the Z_1 and Z_2 dependencies. The impact parameter dependent Firsov model is modified by using the apsis of the collision r_0 instead of the impact parameter suggested by Robinson and Torrens (1974). This change is essential in the case of the collision chains in which the impact parameter is often small. The inelastic energy loss in a single collision is then

$$\Delta E_e = 4.3 \times 10^{-8}(Z_1 + Z_2)^{5/3} v/[1 + 0.31(Z_1 + Z_2)^{1/3} r_0]^5 \tag{7}$$

where ΔE is given in eV if the velocity is measured in cm s^{-1} and r_0 is in Å. The original Firsov model leads to overestimation of energy losses in head-on collisions, because the impact parameter b is very small. On the other hand, this model is not applicable in head-on collisions, because Firsov made an assumption of small angles of

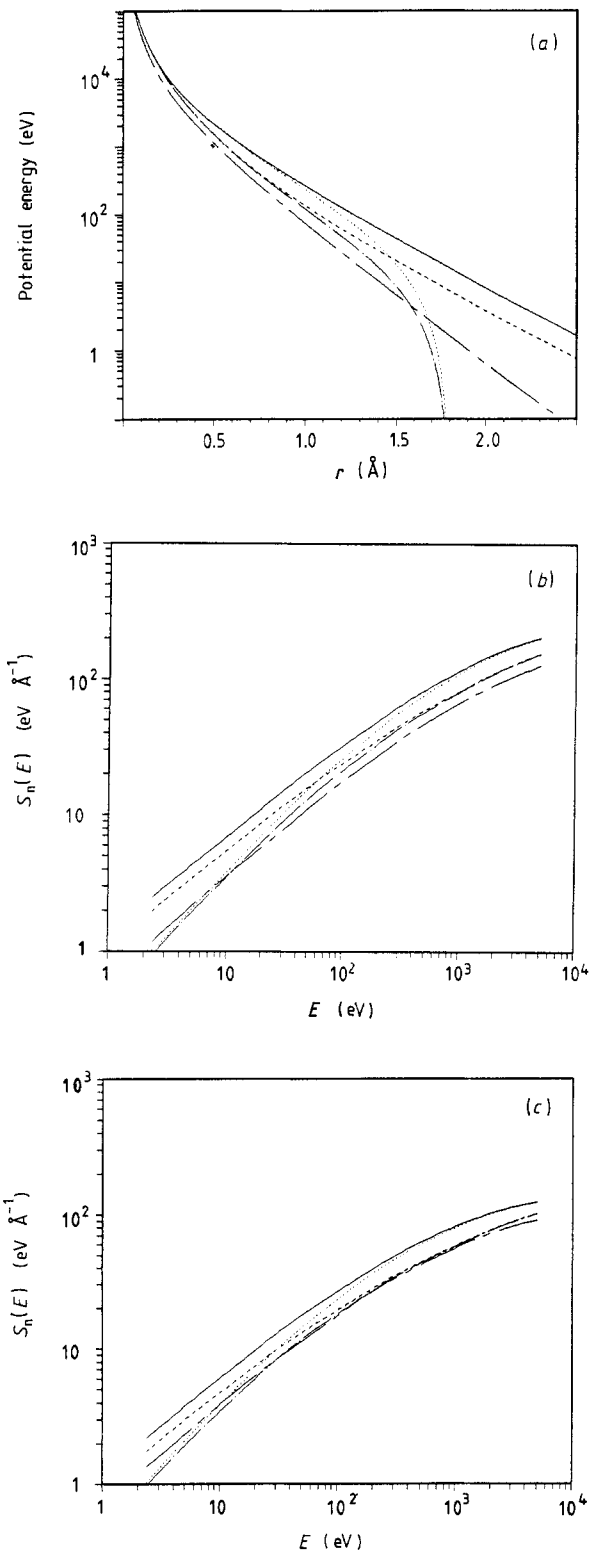

Figure 2. (*a*) Comparison of different potentials for the Cu–Cu interaction, (*b*) nuclear stopping powers for the Cu–Cu interaction and (*c*) nuclear stopping powers for the Ar–Cu interaction. Molière with Thomas–Fermi screening length (_____), mean with Thomas–Fermi screening length (- - - - -), eroded Molière (1) with Thomas–Fermi screening length (.....), eroded mean (1) with Thomas–Fermi screening length (— · —), Molière with Robinson screening length (— - —).

scattering. The modification suggested by Robinson reduces the inelastic losses below the predictions of Firsov, especially at low energies and small impact parameters. The Oen–Robinson energy loss model (Oen and Robinson 1976)

$$\Delta E_e = (0.045kE^{1/2}/\pi a^2)\exp(-0.3r_0/a) \tag{8}$$

is semi-empirical. k is the stopping parameter from the LSS theory. The constant is obtained by demanding that the integrated cross section agrees with (6). This formula was first applied in the case of light ion reflection from metals, but later it was used for other ion–atom combinations, too. The precise form of it was chosen arbitrarily but it seems to give reasonable values of the number of reflected particles as well as their energies in comparison with experiments. It accounts also for the real ion trajectory by considering the closest approach r_0 rather than b. The electronic stopping powers

$$S_e(E) = 2\pi N \int_0^{b_{max2}} b\Delta E_e \, db \tag{9}$$

for the models used are shown in figure 3. In this paper no distinction is made between the ion–atom and the atom–atom pair in the case of inelastic energy losses. In other words, the same model is used for both pairs and the effect of both pairs is not studied separately. It will be shown later in figures 8–10 that inelastic energy losses have only

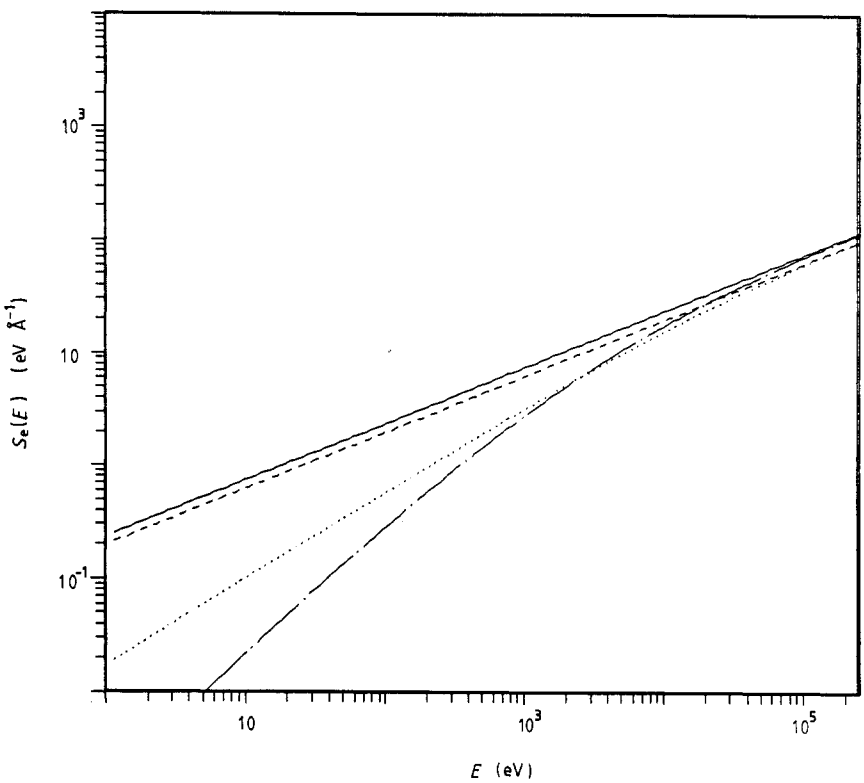

Figure 3. Electronic stopping powers for Cu recoils in Cu in different approximations: Lindhard (_____), Firsov (- - - - - -) , Firsov modified by Robinson (.....) and Oen–Robinson (— · —). In the last two approximations the Molière potential with Robinson screening lengths was used in calculating the apsis r_0 of the collisions.

minor effects on the angular distribution of sputtered particles. However, the yield depends markedly on inelastic losses (Robinson 1983, Biersack and Eckstein 1984) and it has been shown in other computer simulations (Jakas and Harrison 1984) that the atom–atom inelastic energy losses contribute to almost all of the change of the yield, while the ion–atom inelastic energy loss contribution to the change is much smaller. This is quite natural since the fraction of the energy of the incoming ion that goes to electrons is small compared to that going to an atom in an elastic collision. On the contrary, during the collision chains the energy loss to electrons is comparable to that going to remote elastic collisions and therefore the contribution to sputtering is understandable. Thus, although we change at the same time the inelastic energy loss of ion–atom and atom–atom pairs, we do actually study the influence of the inelastic energy loss in atom–atom collisions.

The surface is represented by a planar barrier with the sublimation energy as surface binding energy E_s. The surface binding energies are: 3.5 eV (100), 3.2 eV (110) and 4.1 eV (111) (Yamamura and Takeuchi 1987). Thermal vibrations are included by assuming the displacements to be uncorrelated and Gaussian distributed. The root mean square displacement of the target atoms is based on the Debye model. The target temperature was 300 K in the simulations.

The 5 keV Ar projectile ions are incident along the z direction and impinge on the target surface at normal incidence. The recoils in the cascades are followed until their energy falls below a threshold energy E_c or they reach the surface. The threshold value E_c is chosen equal to the surface binding energy. A target atom is considered to be displaced when recoiling with a kinetic energy larger than a threshold value E_d. E_d is also chosen equal to the surface binding energy. Note that both E_d and E_c are model parameters introduced for numerical convenience and they have no physical meaning.

3. The effect of the parameters in treating the binary collisions

In this section the effect of different model parameters that are significant in binary collision codes in general will be discussed. Some of the parameters discussed later are inherent only in BC codes (e.g. back-up of recoils, maximum impact parameter) and others have real physical meaning (e.g. target temperature). Rather few results have been published on the effect of different model parameters in the case of sputtering and BC calculations.

Table 1. The sputtering yield Y, when one of the parameters is changed, and the standard yield Y_s is 5.2. The potential is Molière with Robinson screening lengths. The standard values of the parameters are: $x_1 = x_2 = 1.5$ Å (maximum values), $\Delta x = 0.4$ Å, $E_b = 0.2$ eV. Oen–Robinson inelastic energy loss is used. The statistical uncertainty is 5%.

x_1 (Å)	Y	x_2 (Å)	Y	Δx (Å)	Y	E_b (eV)	Y
0	5.3	0	5.2	0.1	5.1	0	5.7
0.8	5.3	0.8	5.2	0.7	5.2	0.5	4.6
1.8	5.2					1.0	4.1
						2.0	3.1

The effect of changing the values of some of the input parameters are given in tables 1, 2 and 3, for a Cu(100) surface irradiated at normal incidence. In the case

of table 1 the Molière potential with Robinson screening lengths and Oen–Robinson inelastic energy loss (8) was used, whereas in tables 2 and 3 the screening lengths were Thomas–Fermi. In addition to this, the effect of the simultaneous collisions is studied in tables 2 and 3. In table 2 the simultaneous collisions are omitted and the next scatterer is that target atom which has the smallest impact parameter among the nearest and next-nearest neighbours. In table 3 the simultaneous collisions are taken into account. The maximum values of x_1 and x_2 were limited to 1.5 Å in all standard cases. Robinson and Torrens (1974) have calculated x_1 and x_2 in the case of the Molière potential and head-on collisions. These calculations show that x_1 depends quite strongly on energy and it equals to half of the nearest-neighbour distance 1.28 Å at about $E = 9$ eV. On the other hand, x_2 is quite independent of energy and it is less than 0.5 Å. Thus, the maximum values of x_1 and x_2 in the standard cases are just matters of convenience and only in a few instances they hinder low-energy particles to back up more than the original distance between the collision partners. The yield and the angular distribution for the standard values of the model parameters in table 1 correspond to the results of experiments (Onderdelinden 1968) and other computer simulations with equal parameters (Hou and Eckstein 1986, Yamamura and Takeuchi 1987), although the standard yield is somewhat higher than other results. In tables 2 and 3 the potential is noticeably stronger than in table 1 and thus the effect of the model parameters might be more pronounced than in table 1. In fact, one can observe that the omission of the simultaneous collisions in table 2 leads to an unrealistically high standard yield, whereas the standard yield in table 3 is comparable with table 1. On the contrary, further calculations show that the values in table 1 are insensitive to whether the simultaneous collisions are included or not.

Table 2. The sputtering yield Y, when one of the parameters is changed, and the standard yield Y_s is 27. The potential is Molière with TF screening. Oen–Robinson electronic energy loss is used. The simultaneous collisions are omitted. The statistical uncertainty is less than 10%.

x_1 (Å)	Y	x_2 (Å)	Y	E_b (eV)	Y
0	27	0	24	0	40
0.8	23	0.8	27	0.5	17
1.8	25			1.0	10
				2.0	7.6

Table 3. The sputtering yield Y, when one of the parameters is changed, and the standard yield Y_s is 5.8. The potential is Molière with TF screening. Oen–Robinson electronic energy loss is used. The simultaneous collisions are taken into account. The statistical uncertainty is less than 5%.

x_1 (Å)	Y	x_2 (Å)	Y	Δx (Å)	Y	E_b (eV)	Y
0	4.7	0	5.6	0.1	11.6	0	6.6
0.8	5.3	0.8	5.7	0.7	4.2	0.5	5.4
1.8	5.9					1.0	4.8
						2.0	4.1

The feasibility of the binary collision approximation may be studied best by changing x_1, x_2 and Δx. When the maximum value of x_1 is limited it can be seen

in tables 1, 2 and 3 that the results are rather insensitive to x_1 within statistical uncertainties, except when the back-up of projectiles is totally omitted ($x_1 = 0$). On the other hand, the changes in yields due to different maximum values of x_1 are not systematic. The situation regarding the maximum value of x_2 is quite the same as with x_1. The yields are quite insensitive to variation of the maximum value of x_2. Only when $x_2 = 0$ are the yields somewhat smaller than in the standard cases. Further calculations show that x_1 and x_2 have minor effects on the angular distributions of the sputtered atoms. Only in the cases of $x_1 = 0$ or $x_2 = 0$ are there differences in the distributions. The parameter Δx has practically no effect on sputtering yields and the angular distributions, when the interaction potential is reasonable (see table 1). This is not the case with the stronger interaction potential (see table 3). A small value of Δx produces a high yield, whereas a higher value of Δx gives a reasonable yield. This behaviour reflects the fact that the simultaneous collisions are significant; Δx was a measure of the simultaneous collisions included. A small value of the parameter Δx means that part of the simultaneous collisions in a ring of more or less symmetrically disposed neighbouring atoms are omitted. Higher values of Δx take into account these collisions and also the energy losses in them. These energy losses evidently decrease the sputtering yield. The potentials used in tables 1, 2 and 3 correspond to approximately $0.8a_F$ and $1.1a_F$ respectively in figure 5 below. The simultaneous collisions are not significant when $a = 0.8a_F$ but in the case of $a = 1.1a_F$ the situation is quite the opposite. Thus it can be concluded that the BC approximation is adequate in outlining those low-energy motion problems, which are likely to be significant experimentally.

The bulk binding energy E_b has a large influence on the sputtering yields especially in table 2. In the case of $E_b = 0$ eV the energy losses are underestimated which leads to unrealistically long collision chains and too high sputtering yields. A comparison between binary collision and molecular dynamics calculations shows that $E_b = 0.2$ eV is an appropriate choice for Cu (Robinson 1981). $E_b = 1$ and 2 eV, which are close to vacancy formation energies for FCC metals, give clearly too small yields. In the early MARLOWE simulations the bulk binding energy was either overlooked or totally omitted (Hou and Robinson 1976, 1979, Hou 1981). The effect of the omission of E_b is not discussed in these simulations, but it is probably justified because scattering mechanisms were under study, not development of collision cascades or sputtering. However, taking into account the bulk binding energy improves the treatment of linear collision sequences in BC codes. One way of partly circumventing the problem of choosing the value of E_b is to use the relation $E_b + E_s = H_s$, H_s being the heat of sublimation (Robinson 1981, Biersack and Eckstein 1984). According to Biersack the sputtering yield does not change if this relation is used. The effect of this relation on the angular distribution of sputtered particles is not studied in this paper.

Some calculations were made to study the effect of the target temperature. The sputtering yields were calculated in the temperature range 0–900 K using the Molière potential with Robinson screening lengths and Oen–Robinson inelastic losses. A (100) Cu surface was irradiated at normal incidence. The general tendency was a slight decrease of the yield as a function of the target temperature. This behaviour is to be expected because thermal vibrations hamper a focused transfer of momentum along an atomic row and result in attenuation of focused collision chains. The decrease in yield has been observed in other computer simulations, too (Shulga 1983, 1984, 1985). On the other hand, with increasing temperature the root mean square amplitude of thermal vibrations increases. This causes among others a decrease of the channelling fraction as well as increase of the probability that channelled particles transfer to the

random fraction. In a low index direction these effects lead to an increase of the sputtering yield. This temperature behaviour has been observed experimentally (Elich *et al* 1972).

The yields did not alter significantly when the maximum impact parameter b_{max2} was changed over the range (0.5–0.72)a in the case of the Molière potential with Robinson screening lengths. A small value of b_{max2} lowers the elastic energy loss because collisions with small energy transfer will be omitted. On the other hand, the small scattering angles become larger since the distant simultaneous collisions will be omitted. Larger values produced only small decreases in the yields, but required increased computing time. The decrease of the yield in this case is partly due to Oen–Robinson inelastic loss (8) which depends on the minimum distance r_0 in the collision and hence on the impact parameter. The yield dependence on the maximum impact parameter b_{max2} in the case of the Molière potential with the Thomas–Fermi screening lengths is totally different from the case of the Molière potential with Robinson screening lengths. When $b_{max2} = 0.5a$, most of the simultaneous distant collisions are omitted and the yield is very high ($Y = 15.4$). Larger values of b_{max2} decrease the yield because more and more simultaneous collisions are taken into account and, as already shown earlier, these collisions are very significant. Finally, $b_{max2} = 0.72a$ gives $Y = 5.3$.

It is quite natural that the assumption of the ideal crystal emphasises the role of the ⟨110⟩ chains and thus increases the yield. The collisions occur in every plane and the focusing is very efficient. On the contrary, any distortion (missing atom) rapidly removes the possibility of the chain propagating. A set of calculations, where the surface erosion was left out, was compared with those where it was taken into account. Surface erosion here means the erosion during a collision cascade, not a cumulatitive effect of many cascades. The yields were only slightly higher in the cases where the surface erosion was omitted and the distributions showed practically no deviations. These together with the results of table 4 below indicate that the ideal crystal approximation is good. It is surprising at first sight but as shown in our previous paper (Likonen and Hautala 1988) the probability of a certain target atom being sputtered is rather small. In that paper we studied the origin of sputtered atoms with respect to the impact point of the incoming ion in the case of monocrystalline Cu and these calculations showed very clearly that on the average the maximum of the probability is less than 0.1. The atoms in the first layers have the greatest probability of being sputtered and the probability decreases very rapidly as a function of depth (Sigmund *et al* 1989).

In figure 4 are shown the most noticeable effects of some of the parameters on the distributions of sputtered particles when the Molière potential with Robinson screening lengths and Oen–Robinson electronic stopping is used. A Cu(100) surface is bombarded at normal incidence. The angular distribution in figure 4(*a*) shows four ⟨110⟩ spots and one ⟨100⟩ spot. The position and origin of the ⟨110⟩ peaks have been thoroughly discussed recently (Hou and Eckstein 1986, Yamamura 1987, Likonen and Hautala 1988). This spot pattern has also been observed experimentally (Southern *et al* 1963). In figure 4(*b*) the back-up of projectiles is totally omitted ($x_1 = 0$). As a result, the ⟨110⟩ spots have become more pronounced. The yield is practically the same as in the standard case. The ⟨100⟩ spot has decreased with respect to the ⟨110⟩ spots. In figure 4(*c*) the maximum impact parameter b_{max2} is 1.8 Å. The central ⟨100⟩ peak has increased with respect to the ⟨110⟩ peaks. This is quite expected, because most of the simultaneous collisions with four ring atoms in the case of both rows are omitted and for the ⟨100⟩ row the energy losses to the ring atoms are noticeably greater than for the ⟨110⟩ row. Although most of the simultaneous collisions are omitted there is still some

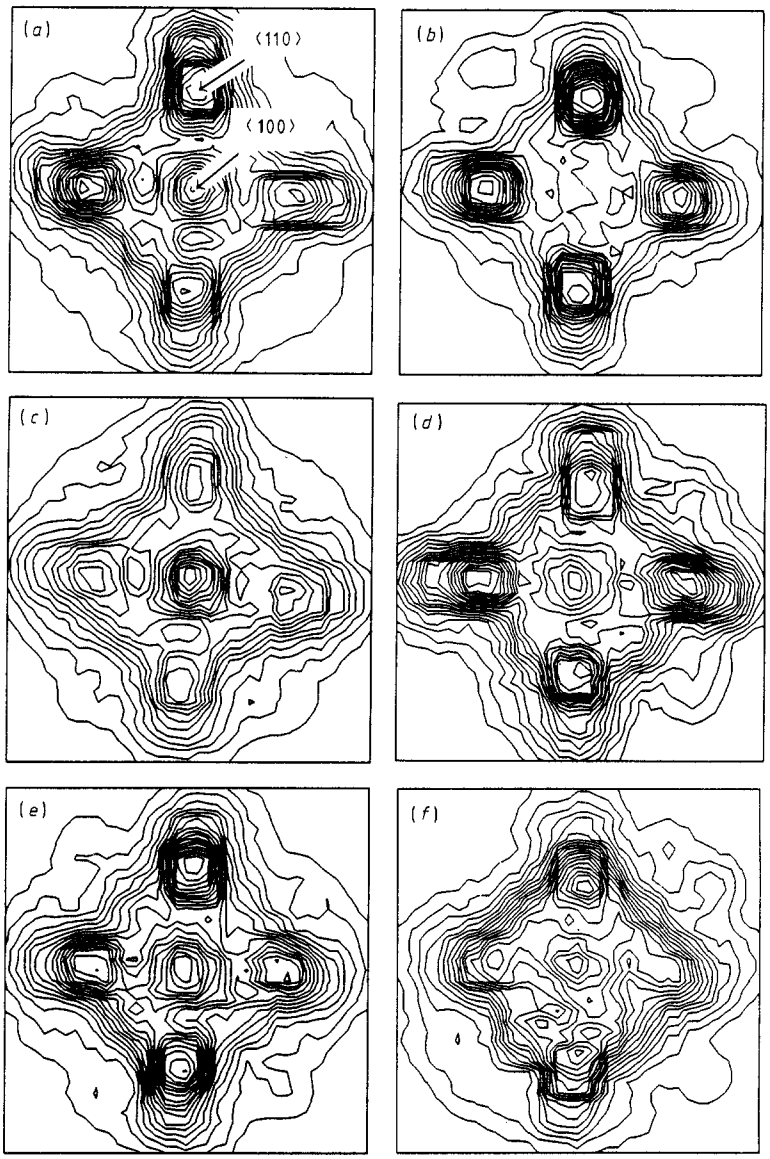

Figure 4. The angular distributions of sputtered particles when the crystal surface is (100) and one model parameter at a time is changed (compare with table 1). (*a*) standard case: $x_1 = x_2 = 1.5$ Å (maximum values), $\Delta x = 0.4$ Å, $E_b = 0.2$ eV, $b_{max2} = 2.25$ Å, (*b*) $x_1 = 0$, (*c*) $b_{max2} = 1.8$ Å, (*d*) $b_{max2} = 2.6$ Å, (*e*) $E_b = 0.5$ eV, (*f*) $E_b = 2$ eV.

assisted focusing left in the ⟨100⟩ rows, but not in the ⟨110⟩ rows. Figure 4(*d*) shows the angular distribution when the maximum impact parameter is 2.6 Å. The distribution is quite the same as in the standard case with $b_{max2} = 2.25$ Å. The ⟨100⟩ peak has decreased slightly with respect to the ⟨110⟩ peaks. In figure 4(*e*) and (*f*) the effect of the bulk binding energy E_b is presented. When E_b is increased, the energy losses of the focused collision sequences are increased. This result can be seen very easily in figure 4(*e*) and (*f*) as the ⟨110⟩ and ⟨100⟩ spots decrease when E_b is increased. The ⟨100⟩

peak has increased with respect to the ⟨110⟩ peaks in figure 4(*f*). This is due to the fact that recoils moving in the ⟨100⟩ direction are more energetic than recoils in the ⟨110⟩ direction. Thus, subtraction of E_b from the kinetic energy affects the propagation of recoils moving in the ⟨100⟩ direction less than the propagation of the ⟨110⟩ recoils.

4. The effect of the interaction potential and electronic stopping on the sputtering yields and the angular distributions

4.1. The yields

4.1.1. Comparison with theory. The effect of the interaction potential on the sputtering yields and the angular distributions is studied by changing the screening length in the Molière potential. A Cu(100) surface is bombarded at normal incidence with 5 keV Ar ions. Figure 5 presents the sputtering yields for the (100) surface when the screening length is varied in the range $(0.6–1.2)a_F$ and the inelastic losses are taken into account by using Oen–Robinson electronic stopping. Figure 5(*a*) shows the yield dependence when both the ion–atom and the atom–atom screening lengths are changed simultaneously. The simultaneous collisions are either included or omitted. Figure 5(*b*) presents the yield in the cases when the ion–atom or the atom–atom screening length is changed at a time and the simultaneous collisions are omitted in both cases. Figure 5(*c*) differs from figure 5(*b*) in the respect that the simultaneous collisions are now included. Generally the yields increase as a function of the screening length. This is due to the fact that the interaction potential is the stronger and the nuclear stopping the larger the bigger the screening length is.

The sputtering yields may be approximated by the Onderdelinden model (Onderdelinden 1968) which can be written as

$$Y(E) = \chi(E)\eta Y_{\text{poly}}(E) \tag{10}$$

where E is the energy of the incident beam. $\chi(E)$ is the non-channelled fraction of the ion beam after entering the crystal surface and η is a fitting parameter. χ is based on Lindhard's channelling theory (Lindhard 1965) and it depends linearly on the ion–atom screening length $a_{\text{Ar–Cu}}$. Y_{poly} is the yield of a structureless medium and according to Sigmund's theory Y_{poly} is (Sigmund 1969)

$$Y_{\text{poly}} \propto S_n(E)/a^2_{\text{Cu–Cu}} \tag{11}$$

where $S_n(E)$ is the nuclear stopping power and $a_{\text{Cu–Cu}}$ the atom–atom screening length. In the LSS theory the reduced nuclear stopping is independent of the screening length. Therefore

$$S_n(\epsilon) = (a'_{\text{Ar–Cu}}/a_{\text{Ar–Cu}})S_n(a'_{\text{Ar–Cu}}/a_{\text{Ar–Cu}}\epsilon) \tag{12}$$

and thus S_n changes a little faster than the screening length $a_{\text{Ar–Cu}}$ and at small energies S_n is approximately proportional to the second power of $a_{\text{Ar–Cu}}$. Thus equation (11) shows that the yield is inversely proportional to the nuclear stopping power of the target atom. The validity of equation (12) is illustrated in figure 6 for Ar–Cu interaction. It

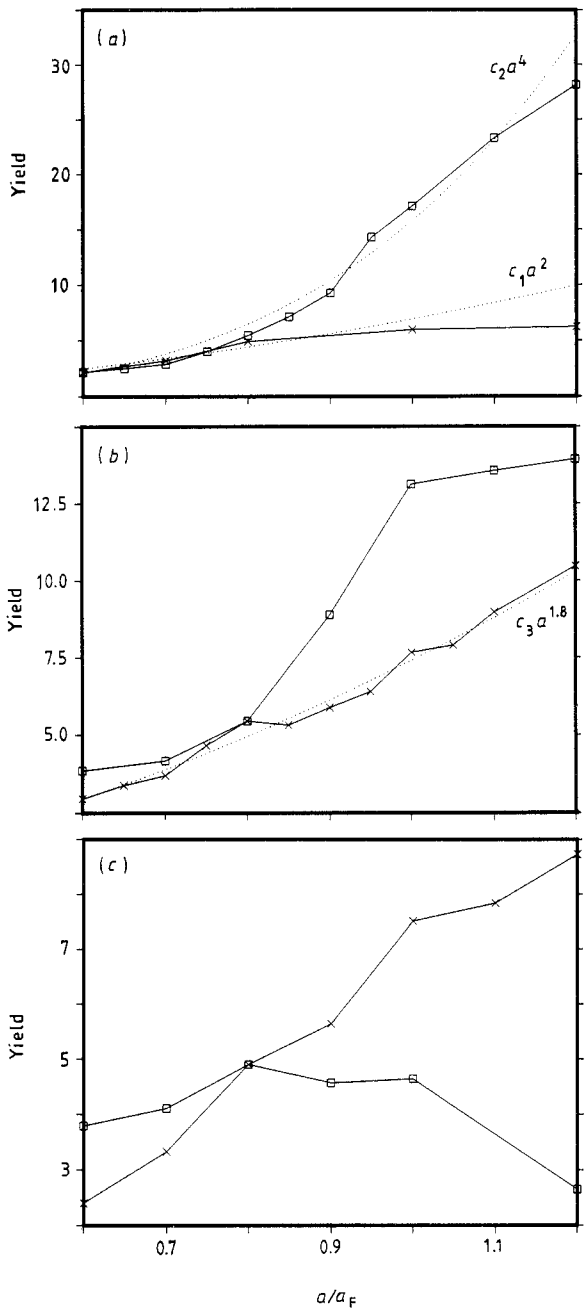

Figure 5. Sputtering yields of Cu atoms sputtered from the (100) surface as a function of the screening length in the Molière potential with Oen–Robinson electronic losses. (*a*) Both Ar–Cu and Cu–Cu screening lengths are changed simultaneously. The simultaneous collisions are included in (×) and in (□) they are totally omitted. a_F is the Firsov screening length. For comparison the best fits to a^2 and a^4 are presented. c_1 and c_2 are fitting parameters. (*b*) Ar–Cu (×, $a_{Cu-Cu} = 0.8a_F$) or Cu–Cu (□, $a_{Ar-Cu} = 0.8a_F$) screening lengths are changed independently. The best fit to $a^{1.8}$ is presented, c_3 is a fitting parameter. The simultaneous collisions are omitted in both cases. (*c*) is the same as (*b*), but the simultaneous collisions are included in both cases.

represents the ratio of the nuclear stopping powers $S_n(a_{Ar-Cu})/S_n(a_F)$, where a_{Ar-Cu} is in the range $(0.6–1.3)a_F$. At energies $E \sim 5$ keV, $S_n(E)$ is proportional to a_{Ar-Cu}. Thus on the basis of equations (11) and (12) one would expect that the yield is approximately proportional to a^2_{Ar-Cu} and inversely proportional to a^2_{Cu-Cu}. Figure 5(*a*) shows that the yields increase approximately to the second power of the screening length when $a = (0.6–0.8)a_F$ and the simultaneous collisions are included or they are omitted. When $a \geq 0.8a_F$ the $\langle 110 \rangle$ spots start to dominate and the yield increases strongly as a function of the screening length when the simultaneous collisions are omitted. A fit shows that the yield dependence is approximately a^4. The yield stays almost constant in the case of the simultaneous collisions included. In figure 5(*b*) the yield is proportional to $a^{1.8}_{Ar-Cu}$ ($a_{Cu-Cu} = 0.8a_F$). Thus, the yield follows equation (11) quite nicely.

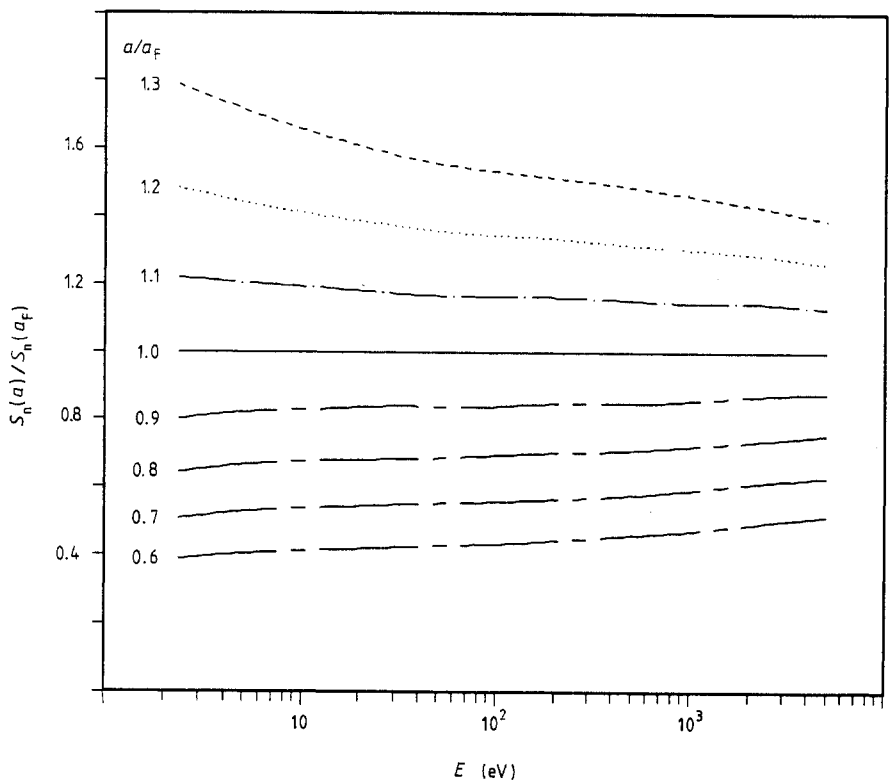

Figure 6. The ratio of the nuclear stopping powers $S_n(a)/S_n(a_F)$ of Ar–Cu interaction as a function of energy. The screening length a is in the range $(0.6–1.3)a_F$.

When the Cu–Cu screening length is changed ($a_{Ar-Cu} = 0.8a_F$), the yield increases strongly and then it reaches a plateau. This plateau is due to the fact that at small energies the nuclear energy losses increase very strongly as a function of screening length according to figure 6. This behaviour is quite the opposite of what is expected on the basis of equations (10)–(12). When simultaneous collisions are included (figure 5(*c*)) the yield rises monotonously as a function of a_{Ar-Cu} ($a_{Cu-Cu} = 0.8a_F$). When the Cu–Cu screening length is increased ($a_{Ar-Cu} = 0.8a_F$), the yield first increases, reaches a maximum and then decreases. This is due to the fact that the simultaneous collisions

act mainly as an energy sink and thus the length of the collision sequences is shortened, although the focusing may be improved. Thus, the energy transfer back to the surface is partly hindered. The increase of yield, when the atom–atom interaction potential is getting stronger, has been observed also in molecular dynamics simulations (Harrison and Webb 1982). The importance of the simultaneous collisions between target atoms can be noticed when figure 5(*b*) and (*c*) are compared with each other. In figure 5(*b*), when $a > 0.8a_F$, the yields are higher for the Cu–Cu curve than for the Ar–Cu curve. The situation is, however, quite the opposite in figure 5(*c*).

Electronic stopping is included implicitly in (11). Some further calculations were made without the electronic energy loss. The effect of the inelastic energy loss is most pronounced in the case of the simultaneous collisions included and Cu–Cu interaction. In this situation the omission of the electronic energy loss increases the yield on the average 15% but the shape of the curve does not change in figure 5(*c*).

The Onderdelinden model combined with Sigmund's sputtering theory predicts correctly only the yield as a function of Ar–Cu screening length, when the simultaneous collisions are omitted. The Onderdelinden model is a rough approximation which neglects the dechannelling. Also the description of the flux profile of the ion beam as a function of depth is very crude. The model may thus easily disregard a slight stopping dependence. Above all the description of the mechanism creating the collision chains, which transfers energy back to the surface and thus increases sputtering yield, is totally neglected. The Onderdelinden equation should be revised by adding a factor which describes the role of chains. It must be pointed out that Onderdelinden's model takes into account only two-body collisions and many-body focusing collisions as well as other correlated collision processes are ignored. An extension to many-body collisions would be possible in Sigmund's theory if adequate expressions for the cross section were available (Sigmund 1969). Thus, it is quite natural that Onderdelinden's model cannot explain the yield as a function of the screening length when the simultaneous collisions are included.

4.1.2. Comparison with other results. The results are further studied in table 4 where the sputtering yields are compared with the experimental data (Onderdelinden 1968) and MARLOWE results (Hou and Eckstein 1986). The incidence angle of Ar ions is varied and the plane of incidence is parallel to the [011] surface direction in the case of the (100) surface. The angles 0° and 30° for the (100) surface correspond to the low-index directions [100] and [211], respectively. The sputtering yield is reduced when particle incidence along these directions due to the channelling. The incidence angles 20° and 55° were chosen because the yield has a maximum in these directions. For the (110) and (111) surfaces the yields were calculated only for normal incidence because there are no results for other incidence angles. The yields are calculated for both the Molière and the mean potential and for the corresponding eroded potentials. The yields are compared with each other in the case of different screening lengths and electronic energy losses.

All the yields correspond well to the MARLOWE results, when the Molière potential is used. The agreement with the experimental results is quite satisfactory. The truncation of the Molière potential gives somewhat different yields, but the changes are not systematic even though the nuclear stopping power of the eroded potential is markedly smaller than for the normal Molière potential especially in the low-energy region (see figure 2). In most cases the yield is higher for the eroded potential since the truncation of the potential at $r_c = 1.8$ Å effectively means that the maximum impact parameter

Table 4. Calculated sputtering yields for various interaction potentials and electronic energy losses. The experimental yields Y_{exp} are from Onderdelinden (1968). The plane of incidence is parallel to the [011] surface direction in the case of the (100) surface. MAR stands for the MARLOWE simulations (Hou and Eckstein 1986). In the case of the Molière potential R means the Molière potential with Robinson screening lengths and Oen–Robinson inelastic losses. E+R is the same as R except that the potential is truncated at r_c = 1.8 Å. F stands for the Molière potential with Robinson screening lengths and the modified Firsov electronic energy loss. In the case of the mean potential LS stands for the mean potential with a_{TF} and the LSS electronic energy loss. E+LS is the same as previous except that the potential is truncated at r_c = 1.8 Å. F stands for the mean potential with a_{TF} and the modified Firsov electronic energy loss.

			Molière potential				Mean potential		
Surface	θ (deg)	Y_{exp}	MAR	R	E+R	F	LS	E+LS	F
(100)	0	4.2	4.6	5.2	5.2	5.3	3.8	3.3	5.3
	20	10.3	13.0	13.5	14.2	13.3	9.1	10.4	12.9
	30	7.3	7.5	8.7	9.3	8.6	6.2	7.0	9.3
	55	—	16.2	17.2	17.6	16.6	12.3	12.3	16.8
(110)	0	2.9	—	3.7	3.0	3.2	2.1	2.6	3.8
(111)	0	9.2	—	10.8	10.9	10.1	6.9	8.2	10.1

b_{max2} is 1.8 Å. Thus, distant simultaneous collisions are omitted. However, as will be seen below, the corresponding angular distributions are totally different (figure 8 (*f*) and (*h*)). The yields for the modified Firsov's electronic energy loss are somewhat smaller than the corresponding results for Oen–Robinson inelastic losses due to higher electronic stopping power (figure 3). The angular distributions agree well with the experimental ones, when these inelastic losses are used.

The mean potential with the Thomas–Fermi screening lengths and the LSS electronic losses produces clearly smaller yields than the Molière potential, even when compared with the Molière potential with Robinson screening lengths and Oen–Robinson electronic energy loss. One can see that the nuclear stopping power of the mean potential with the Thomas–Fermi screening lengths is markedly higher than for the Molière potential with Robinson screening lengths (see figure 2), but the LSS electronic stopping is so much stronger than Oen–Robinson stopping (figure 3) that the yields are smaller for the mean potential. The truncation of the mean potential changes again the yields. For the (100) surface and the incidence angle 0° the truncation lowers the yield, but for other angles and surfaces it produces higher yields, even though the nuclear stopping power is lower for the eroded potential. The mean potential with modified Firsov electronic energy losses gives clearly higher yields than with the LSS electronic stopping power. The angular distributions in the case of the mean potential with the LSS electronic stopping do not correspond so well to the experimental ones as in the case of the Molière potential and the yields are also too small. The mean potential with modified Firsov electronic losses produces almost similar angular distributions as the same potential with Oen–Robinson inelastic losses (see figures 8, 9 and 10(*a*)). However, the experimentally observed ⟨100⟩ peaks are missing in these distributions. It must be pointed out that most of the yields are somewhat higher than the experimental and the MARLOWE results. A better correspondence would have been achieved if the maximum impact parameter b_{max2} had been little bigger, e.g. 2.6 Å. As already stated earlier, the corresponding yield is somewhat smaller which is partly due to the impact

parameter dependent electronic loss.

4.2. The angular distributions

4.2.1. Dependence on the screening length. The contour plots in figure 7 present the angular distributions of the sputtered atoms when the screening length of the Cu–Cu interaction in the Molière potential is varied in the range $(0.6–1.0)a_F$. The screening length for Ar–Cu interaction is $0.8a_F$. Electronic losses are calculated with Oen–Robinson formula. A Cu(100) surface is irradiated at normal incidence. Figure 7(*a*) shows four small ⟨111⟩ peaks and one pronounced ⟨100⟩ peak. When the screening length is increased, the ⟨110⟩ spots become more pronounced with respect to the ⟨100⟩ and the ⟨111⟩ peaks, which can be seen in figure 7(*a*). The ⟨111⟩ peaks have disappeared totally in figure 7(*b*). In addition to these, the position of the ⟨110⟩ spots shifts towards the surface normal as the screening length still increases (see figure 7 (*c*) and (*d*). In the case of the ⟨110⟩ row, where the neighbours are rather far from the axis, the surface scattering is overwhelmed by the refraction due to the planar binding model. When the potential becomes stronger (by increasing the screening length) the effect of the refraction becomes less significant. The decrease of the ⟨110⟩ peaks and the emergence of the ⟨111⟩ and the ⟨100⟩ peaks in figure 7(*a*)–(*c*), when the screening length is decreased, is apparently due to the fact that the energy transfer to next target atom decreases due to the lowered nuclear energy loss and thus some of the collision mechanisms that create the ⟨110⟩ chains do not operate properly. Also, in the low-energy region the energy losses to the ring atoms increase markedly faster for the ⟨110⟩ rows than for the ⟨100⟩ and the ⟨111⟩ rows, when the kinetic energy of recoils decreases (Robinson 1981). On the other hand, the decrease of the screening length lowers the energy losses to the ring atoms and the loss is larger for the ⟨100⟩ chains than for the ⟨110⟩ chains. We also studied the effect of the variation of the screening length in Ar–Cu interaction on the angular distribution of sputtered particles. They turned out to be practically insensitive on the screening length used. The distributions were dominated in all cases by four distinct ⟨110⟩ peaks.

Further calculations show that for the (111) surface the effect of the screening length is quite analogous to the (100) surface. When the screening length is $0.6a_F$, the angular distribution shows small signs of the ⟨110⟩ and ⟨100⟩ peaks. The ⟨110⟩ and ⟨100⟩ peaks start to develop as the screening length is increased. After this, the ⟨100⟩ spots disappear and the ⟨110⟩ peaks become more pronounced. The position of the ⟨110⟩ peaks shifts towards the surface normal in the same way as in the case of the (100) surface. The balance between the surface refraction and scattering is somewhat different from the (100) surface case where the refraction is dominant. For the ⟨110⟩ peaks in the (111) surface the angle between the surface normal and the ejection direction is small and the effect of both refraction and scattering is also small. This leads to a shift that is insignificant. For the ⟨100⟩ peaks in the (111) surface the ejection angle is large and the surface scattering dominates. The results for the (100) (figure 7) and (111) surfaces confirm the fact that the contribution of the ⟨110⟩ collision sequences increases when the interaction potential becomes stronger. In addition to this, one can conclude that the atom–atom collisions are responsible for sputtering mechanisms, whereas the yield reflects strongly the changes in the ion–atom collisions. The atom–atom interactions effect the sputtering yield, too. These results are consistent with molecular dynamics simulations (Harrison 1981, 1982), although Harrison did

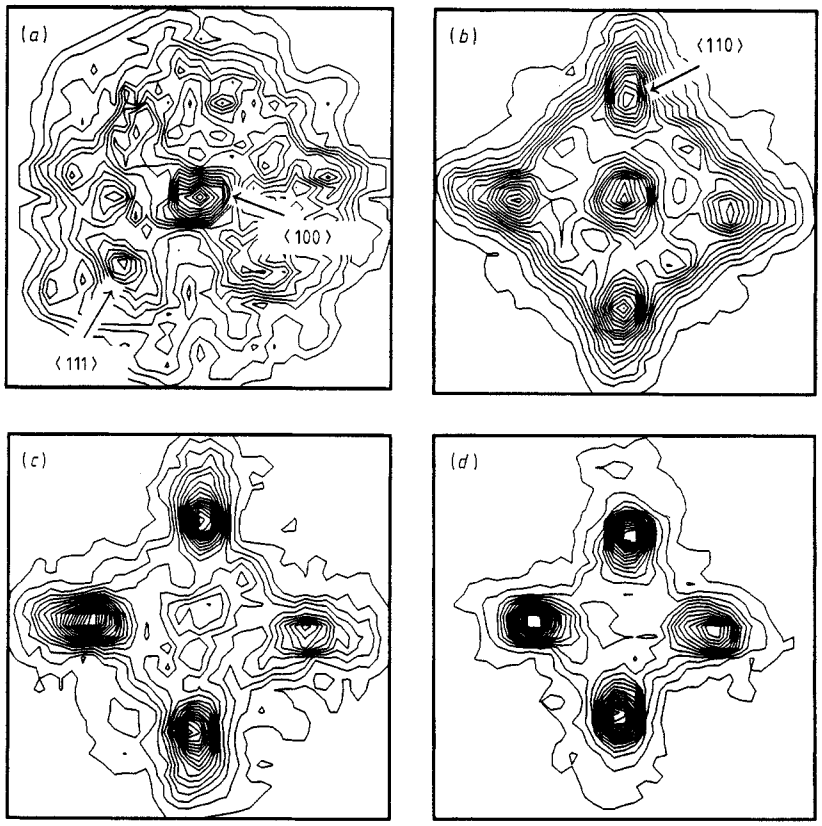

Figure 7. The stereographic projections of the angular distributions of the sputtered atoms when the (100) surface is bombarded at normal incidence with 5 keV Ar. The Molière potential with Oen–Robinson electronic energy loss and $a_{Ar-Cu} = 0.8a_F$ is used. (*a*) $a_{Cu-Cu} = 0.6a_F$, (*b*) $a_{Cu-Cu} = 0.7a_F$, (*c*) $a_{Cu-Cu} = 0.8a_F$, (*d*) $a_{Cu-Cu} = a_F$.

not study the effect of interaction potential on the angular distribution of sputtered particles to a great extent.

4.2.2. Combinations of potential and electronic energy loss: comparison with experiment. The angular distributions of the sputtered particles are compared in figures 8–10 when Cu(100), (110) and (111) surfaces are irradiated at normal incidence with 5 keV Ar ions. The results are shown for the Molière and the mean potentials and also for the corresponding truncated potentials with either the Thomas–Fermi or Robinson screening lengths. Each of these screening lengths is used for both ion–atom and atom–atom interactions. The zero of these truncated potentials occurs at $r_c = 1.8$ Å (see figure 2(*a*)). In figure 8 (*a*)–(*d*) the Thomas–Fermi screening lengths and Oen–Robinson electronic energy loss are used. Both the mean and the Molière potential give four dominant ⟨110⟩ spots (figure 8 (*a*)–(*b*)), whereas in the case of the truncated potentials the ⟨100⟩ spot is greatly enhanced (figure 8 (*c*)–(*d*)). This same effect can also be seen in figure 8 (*e*) and (*g*), where the mean potential with the Thomas–Fermi screening lengths and the LSS electronic energy loss is used as well as in the case of the Molière potential with Robinson screening lengths and Oen–Robinson electronic energy loss (figure 8 (*f*) and (*h*)). The increase of the central ⟨100⟩ peak with respect to

the ⟨110⟩ peaks, when the interaction potential is truncated, is partly due to the same reason that was mentioned in the case of figure 7. When the potential is truncated, the nuclear stopping power decreases as well as the energy losses to the ring atoms. However, as the kinetic energy decreases, the energy losses increase faster for the ⟨110⟩ row than for the ⟨100⟩ row (Robinson 1981). On the other hand, the truncation of the interaction potential at r_c = 1.8 Å effectively means that the maximum impact parameter b_{max2} is 1.8 Å. The enhanced ⟨100⟩spot was already observed in figure 4(*c*), in which the maximum impact parameter b_{max2} was 1.8 Å.

Another feature can be observed when figure 8 (*a*)–(*h*) are compared with each other. Figure 8 can be divided roughly into two groups. In figure 8 (*a*), (*b*) and (*e*) the Thomas–Fermi screening lengths are used and the ⟨110⟩ peaks are the most dominant, whereas in other figures the distributions are clearly different. The differencies in the distributions are connected with the interaction potential and the nuclear stopping power (see figure 2). In figure 8 (*a*), (*b*) and (*e*) the potential and the nuclear stopping power are noticeably stronger than in the other figures. However, when figure 8 (*a*) and (*e*) are compared with each other, the distributions are quite similar. The only difference in the model parameters in these figures is that in figure 8(*a*) Oen–Robinson electronic energy loss is used, whereas in figure 8(*e*) the inelastic losses are from the LSS theory. Thus, one can conclude that the angular distributions depend essentially on the interaction potential and the electronic energy loss has only minor effects. The yield will, however, depend markedly on the inelastic losses (see table 4).

It must be pointed out that in figures 8–10 not only is the atom–atom potential changed, but also the ion–atom potential. However, as already stated earlier, it is the atom–atom potential that is responsible for the angular distribution. The experimental ejection pattern of the sputtered particles shows four ⟨110⟩ spots and one ⟨100⟩ spot in the case of a Cu(100) surface bombarded with 4 keV Ar ions (Southern *et al* 1963). The intensity of the ⟨100⟩ spot is of the same order as the ⟨110⟩ spot. Weijsenfeld (1966, 1967) observed only four ⟨110⟩ spots when a Cu (100) surface was irradiated with 1 keV Kr ions. It can be observed that the Molière potential with Robinson screening lengths and modified Firsov electronic energy loss gives closest agreement with experiment regarding the yield and the ejection pattern (distribution not shown in figure 8). In addition to this, the combination of the Molière potential with Robinson screening lengths and Oen–Robinson electronic energy loss gives also good agreement with experimental results. Other combinations produce either a correct yield or spot pattern.

In figure 9 the angular distributions are further compared in the case of the (110) surface. The parameters of the nuclear and electronic stopping powers are the same as for the (100) surface. One can observe that the differences in various cases are not so pronounced as for the (100) surface. Both the mean and the Molière potential produce a very intensive central ⟨110⟩ peak and four discernible ⟨110⟩ peaks (figure 9(*a*)–(*b*)). The corresponding truncated potentials give somewhat different distributions (figure 9(*c*)–(*d*)). The non-central ⟨110⟩ peaks have become smaller with respect to the central peak and two ⟨100⟩ peaks have emerged. Figure 9 (*e*) and (*f*) show the same features as figure 9 (*a*) and (*b*), though the non-central peaks have become smaller. The truncation of the potential increases again the ⟨100⟩ peaks with respect to the central ⟨110⟩ peak (figure 9 (*g*) and (*h*)). The non-central ⟨110⟩ peaks have almost disappeared.

As already pointed out in the case of the (100) surface, the interaction potential has a major effect on the angular distributions, whereas the electronic energy loss changes only minor details. Experimental ejection pattern from a (110) surface consists

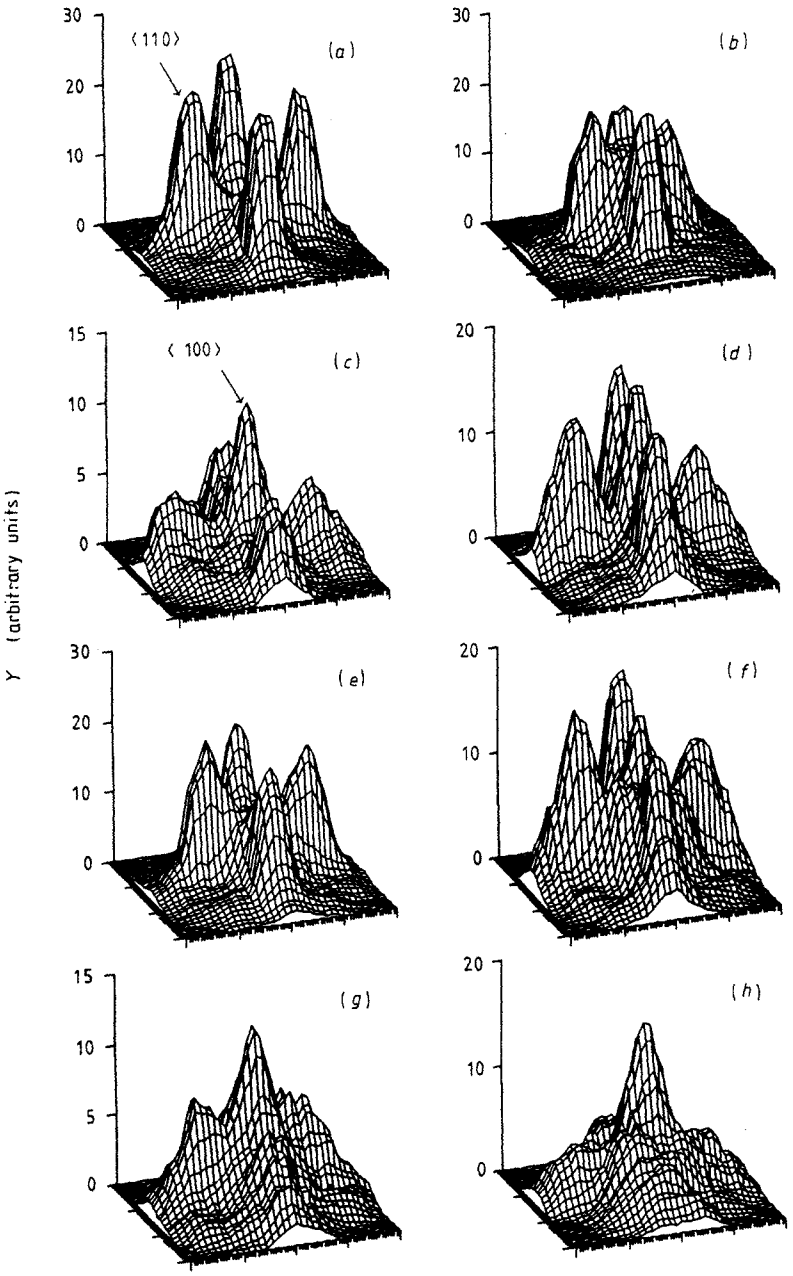

Figure 8. The stereographic projection of the angular distributions of sputtered particles when the Cu(100) surface is bombarded at normal incidence with 5 keV Ar ions. On the left-hand side the potential is mean and on the right-hand side the potential is Molière. In (*a*)–(*d*) Thomas–Fermi screening length and Oen–Robinson electronic energy loss, in (*e*) and (*g*) Thomas–Fermi screening length and the LSS electronic stopping power, in (*f*) and (*h*) Robinson screening lengths and Oen–Robinson electronic energy loss are used, respectively. The potential is eroded in figures (*c*), (*d*), (*g*) and (*h*).

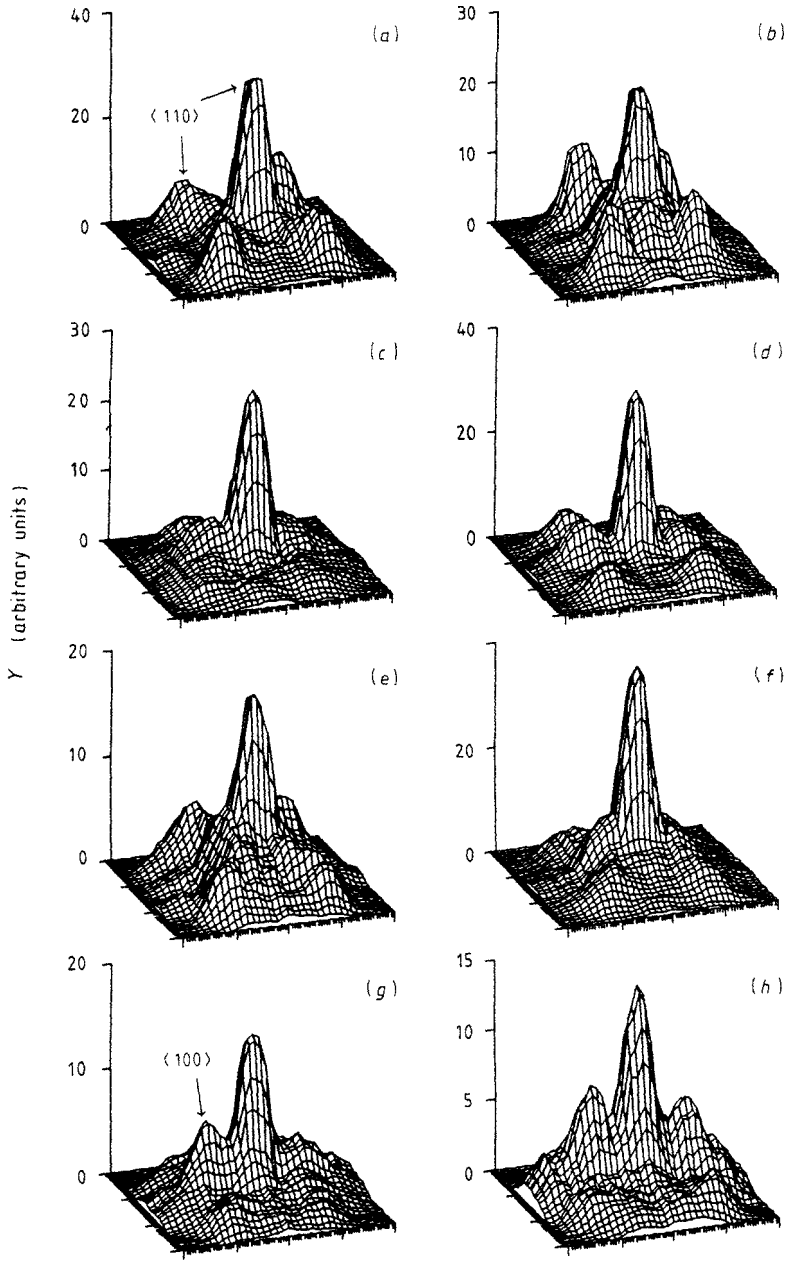

Figure 9. The stereographic projections of the angular distributions of sputtered particles when the Cu(110) surface is bombarded at normal incidence with 5 keV Ar ions. Otherwise as in figure 8.

of an intense central ⟨110⟩ spot, two much weaker ⟨100⟩ spots and four faint spots in the peripheral ⟨110⟩ poles (Southern *et al* 1963). The combination giving both the

yield and the ejection pattern closest to the experimental ones is again the Molière potential with Robinson screening lengths and modified Firsov electronic losses. Also the combinations of the mean potential with the Thomas–Fermi screening lengths and the LSS electronic stopping power and the Molière potential with Robinson screening lengths and Oen–Robinson electronic energy loss (figure 9(*f*)) give results that agree well with the experimental ones.

Figure 10 presents the angular distributions of sputtered particles in the case of the (111) surface. The potential and the inelastic losses are the same as in figures 8 and 9. The differences in the various figures are pronounced, as could also be observed in the case of the (100) surface. The mean potential gives three intense ⟨110⟩ peaks (figure 10(*a*)). The Molière potential produces a central ⟨111⟩ peak and three ⟨110⟩ peaks which have almost become merged in the central peak (figure 10(*b*)). The corresponding truncated potentials modify the patterns somewhat (figure 10 (*c*) and (*d*)). The intensity of the ⟨110⟩ peaks has increased. Three ⟨100⟩ peaks have emerged in the same way as in figures 8 and 9. One can also observe that the position of the ⟨110⟩ peaks is shifted towards the surface when the potential is truncated. In figure 10(*e*) the LSS electronic energy loss, which is markedly stronger than Oen–Robinson inelastic loss, does not change the main features of the distribution when compared with figure 10(*a*). The Molière potential with Robinson screening lengths and Oen–Robinson electronic energy loss gives central ⟨111⟩ and three pronounced ⟨110⟩ peaks (see figure 10(*f*)). There are also three smaller ⟨100⟩ peaks. The truncated potential in figure 10(*g*) increases the ⟨100⟩ peaks in the same way as in figure 10 (*c*) and (*d*). In figure 10(*h*) the central ⟨111⟩ and ⟨100⟩ peaks have increased markedly with respect to the ⟨110⟩ peaks. The electronic energy loss seems again to have only minor effects on the distributions, whereas the interaction potential changes the main features in them. The experimental ejection pattern shows three intense ⟨110⟩ spots, a central ⟨111⟩ spot and three weak ⟨100⟩ spots (Southern *et al* 1963). Again the combinations of the Molière potential with Robinson screening lengths and Oen–Robinson electronic energy loss or modified Firsov electronic energy loss give close agreement with experiment.

5. Concluding remarks

The present paper shows that the binary collision approximation is adequate to reproduce many features in single crystalline sputtering. The results show that binary collision calculations may be used in sputtering studies if adequate carefulness is exercised in interpreting the data. The simulations demonstrate that by suitable selection of the model parameters good agreement with experimental data may be achieved even in the case of angular distributions. However, both sputtering yields and angular distributions and preferably several orientations of crystals must be included in the study if any conclusions of the parameters used are made.

The corrections to the initial position of the asymptotes, the parameter of the criterion for simultaneous collisions and the maximum impact parameter have only minor effects on the sputtering yields and the angular distributions of sputtered particles when the interaction potential is reasonable. If stronger potentials are used, the sputtering yields and the angular distributions are rather sensitive to these parameters. The target temperature and the assumption of ideal crystal produce only slight changes in the sputtering yields. The angular distributions of sputtered particles depend essentially on the interactions between target atoms whereas the inelastic losses and

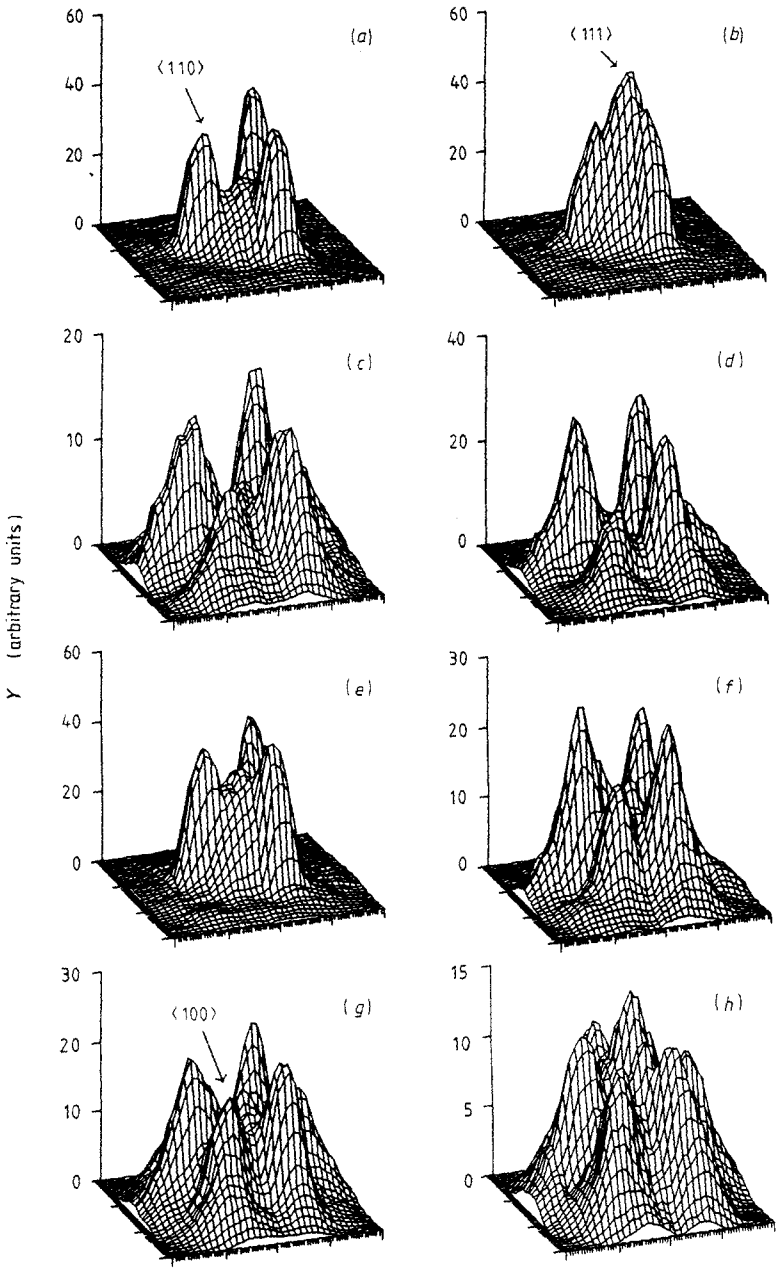

Figure 10. The stereographic projections of the angular distributions of sputtered particles when the Cu(111) surface is bombarded at normal incidence with 5 keV Ar ions. Otherwise as in figure 8.

the ion–atom potential seem to have a minor effect on them. The electronic energy loss has, however, a pronounced influence on the sputtering yields. The effect of the

interaction potential and the simultaneous collisions on the sputtering yields depend substantially on the strength of the potential. Calculations show that this effect is not so significant when the potential produces experimentally observed yields. This is the prerequisite for the binary collision to be a sensible approximation. This may also be the reason for the occasional claims that the BC calculations are not valid for sputtering studies. In fact if unrealistically strong potentials were used or denser cascades were studied this could be true.

The Molière potential with Robinson screening lengths and Oen–Robinson electronic energy loss or modified Firsov electronic energy loss gives closest agreement with experimental results. Other combinations of the screening lengths and inelastic energy losses clearly come out to be inadequate to describe the angular distributions and the yields. In contrast to Biersack's considerations concerning the validity of different interaction potentials (Biersack 1987), the mean potential produces either reasonable yield or angular distribution, not both, at least in the case of sputtering from copper. Recently Eckstein and Hou (1988) have come to the same conclusion when studying sputtering from gold.

References

Andersen H H, Stenum B, Sørensen T and Whitlow H J 1985 *Nucl. Instrum. Methods* B **6** 459
Andersen H H 1987 *Nucl. Instrum. Methods* B **18** 321
Biersack J P and Eckstein W 1984 *Appl. Phys.* A **34** 73
Biersack J P 1987 *Nucl. Instrum. Methods* B **27** 21
Bister M, Hautala M and Jäntti M 1979 *Radiat. Eff.* **42** 201
Eckstein W and Hou M 1988 *Nucl. Instrum. Methods* B **31** 386
Elich J J, Roosendaal H E, Kersten H H, Onderdelinden D and Kistemaker J 1971 *Radiat. Eff.* **8** 1
Elich J J, Roosendaal H E and Onderdelinden D 1971 *Radiat. Eff.* **10** 175
——1972 *Radiat. Eff.* **14** 93
Firsov O B 1959 *Sov. Phys.–JETP* **36** 1076
Fluit J M, Rol P K and Kistemaker J 1963 *J. Appl. Phys.* **34** 690
Harrison D E Jr 1969 *J. Appl. Phys.* **40** 3870
——1981 *J. Appl. Phys.* **52** 1499
——1983 *Radiat. Eff.* **70** 1
——1988 *Crit. Rev. Solid State Sci.* **14** suppl. 1 1
Harrison D E Jr, Levy N S, Johnson J P and Effron H M 1968 *J. Appl. Phys.* **39** 3742
Harrison D E Jr, Moore W L Jr and Holcombe H T 1973 *Radiat. Eff.* **17** 167
Harrison D E Jr and Webb R P 1982 *J. Appl. Phys.* **53** 4193
Hautala M 1984 *Phys. Rev.* B **30** 5010
Hautala M and Likonen J 1987 *Phys. Lett.* **124A** 383
——1988a *Nucl. Instrum. Methods* B **33** 526
——1988b *Phys. Lett.* **131A** 47
Hou M 1981 *Appl. Phys.* **25** 239
Hou M and Eckstein W 1986 *Nucl. Instrum. Methods* B **13** 324
Hou M and Robinson M T 1976 *Nucl. Instrum. Methods* **132** 641
——1978 *Appl. Phys.* **17** 371
——1979 *Appl. Phys.* **18** 381
Jakas M M and Harrison D E Jr 1984 *Phys. Rev.* B **30** 3573
Karpuzov D S 1987 *Nucl. Instrum. Methods* B **19/20** 109
Karpuzov D S and Armour D G 1984 *J. Phys. D: Appl. Phys.* **17** 853
Latta B M and Scanlon P J 1974 *Phys. Rev.* A **10** 1638
Lehmann C and Sigmund P 1966 *Phys. Status Solidi* **16** 507
Likonen J and Hautala M 1988 *Appl. Phys.* A **45** 137
Lindhard J 1965 *Mat. Fys. Medd. Dan. Vidensk. Selsk.* **34** no 14
Lindhard J, Scharff M and Schiott H E 1963 *Mat. Fys. Medd. Dan. Vid. Selsk.* **33** no 14

Magnuson G D and Carlston C E 1963 *J. Appl. Phys.* **34** 3267
Molière G 1947 Z. *Naturforsch.* **2A** 133
Nelson R S and Thompson M V 1961 *Proc. R. Soc.* A **259** 458
Nelson R S, Thomson M W and Montgomery H 1962 *Phil. Mag.* **7** 1385
Oen O S and Robinson M T 1976 *Nucl. Instrum. Methods* **132** 647
Onderdelinden D 1968 *Can. J. Phys.* **46** 739
Robinson M T 1969 *J. Appl. Phys.* **40** 2670
——1981 *Sputtering by Particle Bombardment I* ed. R Behrisch (Berlin:Springer) pp 73–144
——1983 *J. Appl. Phys.* **54** 2650
Robinson M T and Oen O S 1963 *Phys. Rev.* **132** 2385
Robinson M T and Southern A L 1967 *J. Appl. Phys.* **38** 2969
Robinson M T and Torrens I M 1974 *Phys. Rev.* B **9** 5008
Shulga V I 1983 *Radiat. Eff.* **70** 65
——1984 *Radiat. Eff.* **82** 169
——1985 *Radiat. Eff.* **85** 1
Sigmund P 1969 *Phys. Rev.* **184** 383
Sigmund P, Robinson M T, Baskes M I, Hautala M, Cui F Z, Eckstein W, Yamamura Y, Hosaka S, Ishitani T, Shulga V I, Harrison D E Jr, Chakarov I R, Karpuzov D S, Kawatoh E, Shimizu R, Valkealahti S, Nieminen R M, Betz G, Husinsky W, Shapiro M H, Vicanek M and Urbassek H M 1989 *Nucl. Instrum. Methods* B **36** 110
Silsbee R H 1957 *J. Appl. Phys.* **28** 1246
Southern A L, Willis W R and Robinson M T 1963 *J. Appl. Phys.* **34** 153
Weijsenfeld C H 1966 *Thesis* Utrecht
——1967 *Philips Res. Rep. Suppl.* no 2
Wilson W D, Haggmark L G and Biersack J P 1977 *Phys. Rev.* B **15** 2458
Yamamura Y and Takeuchi W 1987 *Nucl. Instrum. Methods* B **29** 461